Title
Direct measurement of velocity space transport in a plasma

Journal
Physics of Plasmas, 1(12)

ISSN
1070-664X

Authors
Bowles, Jeffrey
McWilliams, Roger
Rynn, Nathan

Publication Date
1994-12-01

DOI
10.1063/1.870854

Direct measurement of velocity space transport in a plasma

Jeffrey Bowles,[a] Roger McWilliams, and Nathan Rynn
Department of Physics, University of California, Irvine, California 92717

(Received 6 October 1993; accepted 26 August 1994)

The direct measurement of the velocity space transport of ions in a plasma is reported. Measured diffusion and convection coefficients are compared to the calculated Fokker–Planck coefficients for a fully ionized plasma. The measurements were made in a Q-machine barium plasma ($T_i = T_e = 0.17$ eV, $5\times10^8 \leqslant n \leqslant 8\times10^9$ cm^{-3}) with both high and low fluctuation levels. At low fluctuation levels the measured coefficients agree with classical collision theory. Coefficients measured in the presence of large amplitude fluctuations generally are larger and have different velocity dependences. Test particle distributions are created and interrogated using the technique of optical tagging. The short-time ($\ll 90°$ collision time) relaxation of the test particle distribution function was measured as a function of density and temperature of the background plasma and as a function of the velocity of the test particle distribution. The values of the convection and diffusion coefficients were extracted from these measurements. Longer time relaxations ($\sim 90°$ time) also were measured. © *1994 American Institute of Physics.*

I. INTRODUCTION

This paper develops the previously reported results[1] of the direct measurement of the velocity space transport coefficients made in a fully ionized barium plasma, under conditions close to equilibrium, in a Q-machine.[2] Measurements were made by documenting the evolution of the velocity distribution of a group of test particles along the static confining magnetic field. The test particle distributions were created by optically tagging selected barium ions and then following them for time periods of up to 20% of the ion–ion collision time. Results are presented as the velocity space convection and diffusion coefficients of the Fokker–Planck equation.

Theoretical work applying the Fokker–Planck equation to the plasma state was performed several decades ago.[3] Thereafter the concept of the test particles in a plasma was brought forth.[4–6] The theoretical treatment of collision processes in a plasma made several predictions that could not be directly tested in an experiment at the time. However, recent experimental advances have allowed detailed testing of these theories.

The techniques that have allowed this experiment to be performed include laser-induced fluorescence (LIF)[7] and optical tagging.[8] In the present experiment optical tagging is accomplished by laser-pumping the ground state of the barium ion so as to fill the ion's metastable state. Subsequent "interrogation" by another laser tuned to the metastable transition frequency causes a cascade of electrons back down to the ground state, thereby emitting photons which can be detected; for more details see Ref. 8. Optical tagging has been used to make several transport measurements. Among these are: spatial cross field ion transport in both and quiet turbulent plasmas,[9] spatial ion transport resulting from stochastic wave–particle interaction,[10] ion phase space orbits in the presence of ion-acoustic waves,[11] and the effects of neutral particles on spatial cross field ion transport.[12] Fokker–Planck theory has also been checked in pure electron plasmas.[13]

The Q-machine is described in Ref. 2. Briefly, it consists of a plasma column, singly ionized barium in this case, that is formed by contact ionization on an incandescent rhenium (in this case) surface that also emits electrons. The plasma column is confined radially by a strong magnetic field and terminates on a cold plate opposite the hot ionizing plate. Barium neutrals are removed from the system by chilling the vacuum chamber walls. The result is a low temperature, fully ionized (very few barium neutrals remain in the plasma in the area of the measurements) plasma column with equal ion and electron temperatures of the order of 0.2 eV, with minimum inherent fluctuations. Base pressure in the machine is approximately 2×10^{-6} Torr. We describe the experimental procedure first and then develop comparisons with theory. We discuss a numerical modeling of ion transport performed to explain some aspects of our results in the Appendix.

II. EXPERIMENTAL APPARATUS AND METHODS

The experiments were carried out in the University of California, Irvine (UCI) Q-machine.[2] The ions were accelerated by the sheath in front of the hotplate and then drifted at a speed that was typically 7×10^4 cm/s. The plasma column was 1.4 m long and 5 cm in diameter. Typical densities were 5×10^8 to 8×10^9 cm^{-3}. The density was measured using a Langmuir probe and also was inferred from measuring the angle of the resonance cone of propagation of a lower hybrid wave[14–16] ($\omega_{ci}, \omega_{pi} \ll \omega \ll \omega_{pe}, \omega_{ce}$). The density measured with the latter technique usually gave a somewhat lower value than that obtained from probe measurements. The ion temperature and drift speed were derived from ion velocity distributions measured by using LIF with a procedure that we will describe briefly.[7] Singly ionized barium has several optical transitions in the visible region that make barium plasmas an ideal candidate for optical measurements (see Fig. 1). In order for a barium ion to absorb a photon the Doppler relation,

[a]Present address: Naval Research Laboratory, Plasma Physics Division, Code 6756, Washington, D.C., 20375.

 1070-664X/94/1(12)/3814/12/$6.00

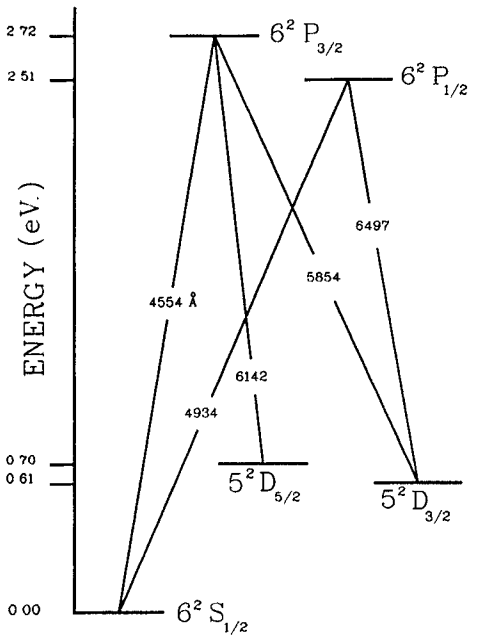

FIG. 1. Shows the various levels of the barium ion. The wavelengths of the transitions are shown.

$$\omega = \omega_0 - \mathbf{k}\cdot\mathbf{v}, \tag{1}$$

must be satisfied. Here ω is the measured frequency, ω_0 is the transition frequency of a stationary ion, $\mathbf{k}$ is the wave vector of the incident photon and $\mathbf{v}$ is the velocity of the ion in the lab frame. The laser–ion interaction selects only the component of the ion's velocity which is parallel to the direction of propagation of the laser beam ($\hat{\mathbf{k}}$). In the process of absorbing a photon the ion is excited to a state which has a very short lifetime (~10 ns). A photon is emitted as the excited ion decays to a lower energy state. The frequency of the emitted and absorbed photons are not necessarily the same. Thus, all results are effectively integrated with respect to the two directions perpendicular to the beam direction. By using a scannable, single-mode tunable dye laser it is possible to scan the Doppler broadened absorption line of the singly ionized barium ion yielding the ion velocity distribution directly. For more details see the reference by Hill *et al.* [7] The frequency of the lasers can be scanned as much as 30 GHz. However, scans between 5 and 12 GHz usually were used. The full width at half maximum (FWHM) of the Doppler broaden absorption spectrum of the ions, at a temperature of 0.2 eV, is approximately 1 GHz (this number changes slightly depending on which transition is used). The velocity resolution is roughly 0.02 v_{th} at T_i=0.2 eV. In the presence of a magnetic field singly ionized barium is subject to anomalous Zeeman splitting. The field splits the degeneracy resulting in the levels splitting into either 2 (the $6^2S_{1/2}$ and $6^2P_{1/2}$ levels) or 4 (the $5^2D_{3/2}$ and $6^2P_{3/2}$ levels) distinct levels. The measured velocity distribution appears as a series of partially overlapped distributions which makes interpretation more difficult. However, the transitions between the levels are sensitive to the polarization (relative to the magnetic field) of the photons. This allows the overlaps to be reduced by the use of polarizing filters on the laser beam and the light emitted from the plasma. Also the experiment was performed at 5 kG. At this field strength and with the use of filters there is enough separation of the levels to prevent overlap. The Zeeman effect does not negatively impact the interpretation of the results of this experiment. The parallel velocity distribution is measured by directing the laser light into the plasma in the axial direction. The drift velocity is measured by comparing parallel and perpendicular distributions. Since there is no perpendicular drift velocity, perpendicular velocity distributions are centered at zero drift (which was verified by sending the laser beam through the center of the plasma column at different angles; the parallel direction of the laser beam cannot be reversed because the plasma source is located at one end). A frequency shift will be seen between the peaks of the perpendicular and parallel scans. The corresponding velocity shift may be calculated from $v_{\text{drift}}=\lambda\,\delta\nu$ where $\delta\nu$ is the shift in frequency between the two scans and λ is the wavelength of the laser light.

The idea behind optical tagging (OT) is to mark, by optical means, a group of particles, then allow them to interact with their environment, and then to interrogate the particles. The information thus obtained is determined by the conditions at the tagging point, or time, by the particle–plasma interaction during its transition to the interrogation point, and by the laser beam spectral width and its orientation with respect to the plasma and magnetic field. Using this technique, transport of particles in phase space due to particle–particle interactions or to wave–particle interactions may be measured. Commonly, optical tagging[8] depends on having two optically connected long-lived states. The barium ground state is long lived. From measurements on the Q-machine[9] and other independent measurements[17] the $5^2D_{3/2}$ metastable state of the barium ion has a lifetime much larger than the transit time of an ion through the machine for these experiments. Figure 1 shows the two states used in our measurements. A laser tuned to the 4934 Å transition can move a fraction of the particles in the laser beam path from the ground state into the metastable state. At the interrogation point the metastable transition may now be probed for an increase in level population indicating the presence of tagged particles. This method is termed "bright-pulse" tagging because tagged particles now appear as an increase in the light signal from the metastable transition. A variation of this method has been used by Skiff,[18] which takes advantage of the different spin orientations of the Zeeman components which he has termed "spin-flipped tagging." Figure 2 shows the setup used for the tagging experiments. Measurements of the ion transport, ion temperature, density and density fluctuations were all made in the same local volume. Axial tagging and searching beams were made to overlap spatially by the use of a 50% beam splitter. The beams traversed the plasma axially from the cold collector to the hotplate. Usually, laser pulse lengths of 10 μs were used. The tagging beam was set to excite the 4934 Å line while the search beam excited the 5854 Å line. The beams were 8 mm in diameter (this is approximately 8 Larmor radii). The usual solid cold endplate was replaced by a 100 lines-per-inch cop-

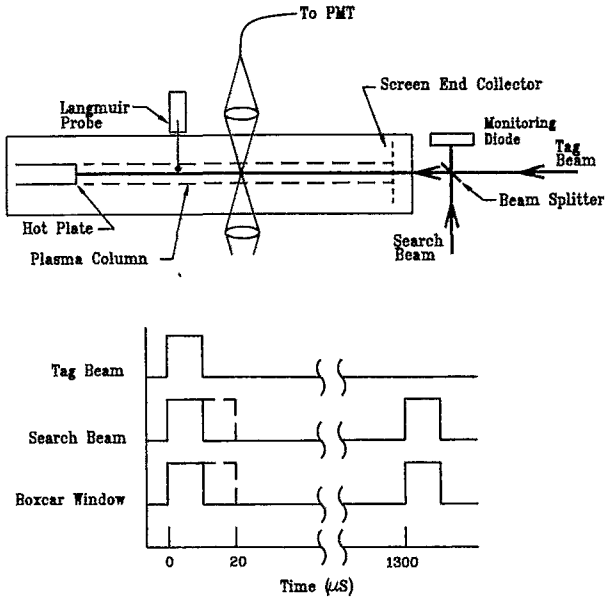

FIG. 2. Setup for tagging experiments as explained in the text. Inset shows the pulse sequence used for tagging measurements. Note the background subtraction used to remove particles naturally occurring in the metastable state. This leaves a signal only from the tagged particles.

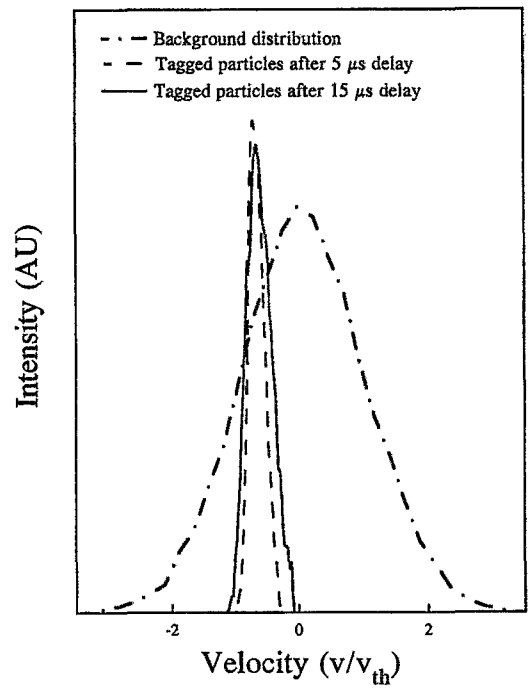

FIG. 3. The figure shows the distribution of the background plasma and two distributions of the tagged particles.

per grid. This was the smallest grid size that could be used without substantial deterioration in laser beam quality. Optical collection devices were located 75 cm downstream from the hotplate. These devices were constructed of achromatic lenses and were designed to focus the collected light onto an optical fiber which then directed the light to a photomultiplier tube (PMT). As will be discussed shortly, there is reason to keep the tagged particle population to a small percentage ($\approx$1%) of the total density. It is possible to estimate the percentage of particles that were tagged. During the ionization process the ions come into thermodynamic equilibrium with the hotplate. Therefore, it is possible to use the Saha equation to estimate the population of the metastable levels. It is estimated 12% of the ions leaving the hotplate were in the $5^2D_{3/2}$ state. This metastable state splits into four sublevels in the magnetic field. This results in 3% of the particles in each sublevel. The percentage of tagged particles can be estimated by comparing the area under the curve of a full velocity distribution of this state (representing 3%) to that of the tagged particle distribution (for example see Fig. 3). During the experiment the highest tagged particle percentage that was seen was 1.5% of the background plasma density.

The tagging procedure was as follows: A full scan of the 4934 Å transition was taken, which provided an ion distribution function measurement. Then a particular velocity (laser frequency) was selected for the 4934 Å transition and it was held steady. The pulse sequence shown in Fig. 2 was used and the 5854 Å transition was scanned. Output from the PMT monitoring the 4554 Å fluorescence, produced by the metastable state excitation, was then used as the input to a boxcar averager. In addition to the tagged particles that have been moved to the metastable state there are also particles naturally occurring in this state. These background particles are also fluoresced by the search beam. To differentiate between the background and tagged particles, the boxcar was run using background subtraction. The output, consisting of the tagged-particle signal only, from the boxcar was then recorded. Figure 3 shows the results of such a measurement. The figure shows a background scan and scans of the tagged particles at two different times. Note that in this example the changes in the average position and the FWHM of the two tagged distributions are clearly visible. However, only the change in FWHM of the distribution is significantly larger than the possible errors. The errors that give rise to errors of measurement of the average position are discussed below. The method of interpretation of the data is described below.

It is important to know the velocity resolution of the LIF and OT techniques. As noted previously an ion may absorb a photon if the Doppler relation is satisfied. However, ω_0 has an intrinsic width, due to radiation broadening which determines the "natural" or "homogeneous" linewidth. This is the smallest width possible and defines the absolute limit of the velocity resolution possible using LIF. The other broadening process most relevant to this work is that of power broadening. Pappas *et al.*[19] give the effective frequency width of the laser beam as

$$\gamma_{\text{effective}} = \gamma\sqrt{1 + I/I_1} \tag{2}$$

where

$$I_1 = \frac{\hbar\omega}{\sigma_0\tau}\left(\frac{1+\tau/T}{2+\Gamma T}\right) \tag{3}$$

and

$$\sigma_0 = \frac{8\pi k \mu^2}{\hbar \gamma}.$$

Here $\hbar\omega$ is the photon energy, τ is the lifetime of the excited state, Γ is the spontaneous emission rate from the excited state to a particular lower state (1×10^8/s for the ground state), μ is the electric dipole matrix element of the transition, γ (typically $\geqslant$20 MHz) is the linewidth of the transition, and T is the ion transit time or time the ion stays in the physical extent of the laser beam. Typically, T is 10 μs and τ is less than 10 ns. For the $6^2S_{1/2}$ to $6^2P_{1/2}$ transition, which has a wavelength of 4934 Å, the natural linewidth is approximately 1000 cm/s. (In our case it is more convenient to discuss resolutions in velocity units to facilitate comparisons with ion velocities as opposed to frequency which may be preferable in other contexts. The conversion is given by $\delta v = \lambda\, \delta\nu$ where λ is the laser's wavelength.) During the experiment power levels of 5 mW/cm^2 for this transition were typically used giving a power broadened linewidth of 2100 cm/s, roughly twice the natural wavelength. For the $5^2D_{3/2}$ to $6^2P_{3/2}$ transition, which has a wavelength of 5854 Å, the natural linewidth is 1500 cm/s. Power levels were typically 10 mW/cm^2 resulting in an effective linewidth of 2700 cm/s, less than twice the natural wavelength. The tagged particle distributions are measured using the metastable state transition and have a FWHM of typically 18000–21000 cm/s and the base of the distribution is roughly twice that. This means there are approximately 15 points to distinguish the Maxwellian shape. Fifteen points is enough to distinguish the Maxwellian shape however, deconvolution of the measurements may give a more accurate measurement of the test particle distribution function. The transport measurements depend on comparison of two distribution measurements. Deconvolution of the distributions would change both distributions approximately the same amount thus deconvolution appears unnecessary. Since the background distribution is wider than the test particle distributions the effect of power broadening is correspondingly less. Furthermore, there is reason to believe that the model overestimates the power broadening effect. Since a typical value of τ is 10 ns, Γ is 10^8, and T, the pulse length, is 10 μs, the numerator of Eq. (3) is approximately 1 and the denominator is ΓT. This results in equation I_1 being proportional to $1/T$. The model assumes that the particle's velocity is within the Doppler broadened linewidth for its entire time in the beam. However, some particles will diffuse out of the velocity range covered by the laser spectral width during the transit time. In fact, from the value of the diffusion coefficients ($\approx10^{12}$ cm^2/s^3) the estimated length of time ($t\approx\gamma^2/D$) that an ion's velocity may be within the laser linewidth is 1 μs. Thus the effective T may be less than 10 μs and $\gamma_{\text{effective}}$ may be lower than stated above.

III. THEORY CONCERNING VELOCITY SPACE TRANSPORT

The theory concerning collisional velocity space transport has a long history. Theoretical work on extending the Fokker–Planck equation to plasmas was accomplished by Rosenbluth *et al.*[3] The calculation of long time relaxation of test particle distributions was performed by MacDonald *et al.*[20] The concept of the test particle in plasmas was extended by Thompson[5] and Rostoker.[6] It is the concept of the test particle that is the cornerstone of the experiment presented in this paper. A more complete list of references concerning collisional velocity space transport in a plasma may be found in an article by Hinton.[21]

The ideal test particle is distinguishable from all other particles, called field or background particles, yet behaves the same as all other particles in every respect. The ability to distinguish the test particle allows the test particle's path to be followed in phase space. The test particle's path is determined by collisions with the background particles and any external fields present. The only moment of ambiguity would be during the collision of one test particle with another when, after the collision, one would not be able to determine which was the initial particle. By keeping the test particle population down to about one percent of that of the field particles, the interaction among test particles is negligible compared to that between field and test particles, and the transport measurements are not compromised. The signal-to-noise ratio is significantly enhanced by having more than one test particle in the interrogation volume.

A plasma may be characterized concerning the role of collisions in the plasma by considering the Coulomb coupling constant, Γ,[22] which is the ratio of the average potential energy density to the average kinetic energy, and is given by

$$\Gamma = \frac{(Ze)^2/a}{\kappa T}.$$

Here Z is the ion charge number, e is the electron charge, a is the Wigner–Seitz radius (the radius of a sphere corresponding to the average volume per particle given by $1/n$ where n is the density), k is the Boltzmann constant, and T is the temperature. In Q-machine plasmas the value of Γ is approximately 10^{-5}, meaning that the plasma is weakly coupled. Additionally, this means that the particles are for the most part free particles and that the energy exchanged during each collision is small in comparison to the particles' original energy. Only small angle, binary collisions are of importance.

In the calculation of the expected behavior of the test particles no magnetic field is considered. Although the plasma is immersed in a magnetic field the only results presented are measurements made along the field lines. Additionally, in the present work spatial variations in field particle or test particle density are not considered (this aspect is discussed further in Sec. IV). Thus, the Fokker–Planck equation[3] may be used to predict the future of the test particle distribution;

$$\frac{\partial f_T}{\partial t} = -\frac{\partial}{\partial \mathbf{v}} f_T\left\langle \frac{\Delta \mathbf{v}}{\Delta t} \right\rangle + \frac{1}{2}\sum_{i,j} \frac{\partial^2}{\partial v_i \partial v_j}\left(f_T \left\langle \frac{\Delta v_i \Delta v_j}{\Delta t} \right\rangle \right). \tag{4}$$

Here f_T represents the test particle distribution. Equation (4) has been explicitly written to predict the evolution of the test

particle distribution. The coefficients of Eq. (4), summed over the distribution functions of all field particles, and are given by

$$\left\langle \frac{\Delta \mathbf{v}}{\Delta t} \right\rangle = \frac{1}{\Delta t} \int P f_f(v,t)\, \Delta \mathbf{v}\, d(\Delta \mathbf{v}), \tag{5}$$

$$\left\langle \frac{\Delta v_i \Delta v_j}{\Delta t} \right\rangle = \frac{1}{\Delta t} \int P f_f(v,t), \Delta v_i\, \Delta v_j, (\Delta \mathbf{v}), \tag{6}$$

and are called the velocity space convection and diffusion coefficients respectively with f_f representing the field particle distributions.

It remains to express the Fokker–Planck coefficients [Eqs. (5) and (6)]. The derivation may be found in many references.[3,4,23,24] When these coefficients are known the future course of the distribution function f_T is known.

Rostoker and Rosenbluth[4] provide the coefficients:

$$\langle \Delta v_i \rangle_T = \sum_f \frac{4\pi e^4 \ln(\lambda)}{m_T} \left(1 + \frac{m_f}{m_T}\right) \frac{\partial}{\partial v} \frac{1}{4\pi} \int \frac{f_f(\mathbf{v}')}{|\mathbf{v}-\mathbf{v}'|}\, d\mathbf{v}', \tag{7}$$

$$\langle \Delta v_i \Delta v_j \rangle_T = \sum_f \frac{4\pi e^4 \ln(\lambda)}{m_T} \frac{\partial^2}{\partial v_i \partial v_j} \times \left(\frac{1}{4\pi} \int |\mathbf{v}-\mathbf{v}'| f_f(v')\, d\mathbf{v}' \right), \tag{8}$$

where the subscripts T and f refer to the test particles and the field particles respectively.

The convection and diffusion coefficients may now be found by taking moments of Eq. (4). Taking the initial velocity of the test particle in the z direction and the initial test particle distribution as a delta function in velocity, the convection and diffusion coefficients may be written as

$$C_{v_z} = \left\langle \frac{\delta v_z}{\delta t} \right\rangle_T = \frac{-2\pi n e^4 \ln(\Lambda)}{m_T} \sum_f \left(\frac{1}{m_f} + \frac{1}{m_T} \right) \times \frac{\partial}{\partial v_z} \frac{1}{v_z} \operatorname{erf}\left(\frac{v_z}{\sqrt{2} v_{\mathrm{th},f}} \right) \tag{9}$$

and

$$D_{v_z v_z} = \left\langle \frac{\delta v_z \delta v_z}{\delta t} \right\rangle = \frac{-8\pi n e^4 \ln\Lambda}{m_T^2} \sum_f \frac{v_{\mathrm{th},f}^2}{v_z} \frac{\partial}{\partial v_z} \frac{1}{v_z} \operatorname{erf}\left(\frac{v_z}{\sqrt{2} v_{\mathrm{th},f}} \right). \tag{10}$$

Here $v_{\mathrm{th},f} = \sqrt{\kappa T_f / m_f}$ is the thermal velocity of the field particles and the sum is over all field particles.

The data (an example is shown in Fig. 3) are interpreted in terms of the one-dimensional velocity space continuity equation given by

$$\frac{\partial f_T(v_z)}{\partial t} + \frac{\partial \Gamma}{\partial v_z} = 0$$

where Γ is the flux of a velocity element. In line with the previous theoretical discussion, the flux is taken to be composed of a convection contribution and a diffusion contribution. The above equation can then be written

$$\frac{\partial f_T(v_z)}{\partial t} + \frac{\partial}{\partial v_z} \left(C_{v_z} f_T(v_z) + \frac{\partial}{\partial v_z} D_{v_z v_z} f_T(v_z) \right) = 0. \tag{11}$$

Here the coefficients, C_{v_z} and $D_{v_z v_z}$, are one dimensional since we are looking at the change in the z-component of velocity only.

The convection and diffusion coefficients, Eqs. (9) and 10, are not strong functions of velocity (see the theory lines in Figs. 6 and 7). For a specific group of test particles with similar initial velocities, the convection and diffusion coefficients will be approximately the same for all the test particles initially. Hence, for short times the coefficients may be treated as constants for this specific group, making an analytic solution possible. If a considerable amount of time has elapsed between the tagging and searching beams then the particle's phase space trajectory is influenced by the changing values of the transport coefficients. In this case the coefficients cannot be treated as constants and it appears a numerical method is necessary to solve the equation.

In order to find the short-time analytic solution for $f(v_z,t)$ Eq. (11) is Fourier transformed in the velocity variable. The initial condition is taken as a Gaussian distribution of width σ_T. The Fokker–Planck theory was derived using a delta function as the initial condition. However, to facilitate comparison with the experiment a Gaussian distribution is explicitly used here. There is no contradiction here since a delta function can be written as a Gaussian distribution in the limit in which σ goes to zero. A Gaussian was used because it is mathematically simpler and because in the experiment a Gaussian distribution of tagged particles is formed. In the end the interpretation of the experimental results does not depend on the width of the initial Gaussian. The final solution is given by

$$f_T(v_z,t) = \frac{n_T}{\sqrt{2\pi}} \frac{1}{\sqrt{\sigma_T^2 + 2D_{v_z v_z} t}} \times \exp\left(\frac{-(v_T - v_z - C_{v_z} t)^2}{2(\sigma_T^2 + 2D_{v_z v_z} t)} \right). \tag{12}$$

The tagged-particle distribution retains its Gaussian shape but now has time dependent first and second moments given by

$$\langle v_z \rangle = v_T - C_{v_z} t, \tag{13}$$

$$\langle v_z^2 \rangle = \sigma_T^2 - 2D_{v_z v_z} t. \tag{14}$$

By measuring the tagged particle distribution at different times, the above equations can be solved to obtain values of both the diffusion and convection coefficients. Additionally, the second moment can be related to the FWHM of the distribution if it is approximately Maxwellian. By replacing

$\langle v^2 \rangle$ in Eq. (14) with a term for the second moment of a Maxwellian distribution an expression for the diffusion coefficient can be found to be

$$D_{v_z v_z} = \frac{1}{2\Delta t}\frac{1}{5.54}\Delta(\mathrm{FWHM}^2) \tag{15}$$

where $\Delta(\mathrm{FWHM}^2)$ is the change in the square of the FWHM of the distributions and Δt is the time between measurements.

The longtime relaxation of the test particle distribution may be characterized by Eq. (11). However, an analytic solution accurate for long times appears to be very difficult. Instead, an approximate numerical method was used for this case. The details of the numerical method are discussed in the Appendix.

IV. EXPERIMENTAL RESULTS

In the present work the data generally are in two forms that can be called the "short-time" and "long-time" data. One way to reference the relevant time scales is to use Eqs. (13) and (14) to calculate times for the tagged particle distributions to reach halfway to equilibrium. Although these equations were calculated for the short-time scale regime they will give an initial rate at which the test particle distribution approaches equilibrium. The times, t_d for diffusion and t_c for convection, for typical experimental conditions are 80 μs and 600 μs respectively. The time between the beginning of the tagging beam and the beginning of the search beam will be called t_m. The short-time data had values of t_m of between 0 and 10 μs (much less than t_d and t_c). The long-time data had values of t_m in a range between 10 and 160 μs (comparable to t_d but still less then t_c).

The short-time data used the shortest possible pulse sequence. Thus, the measurement reflects the local values of diffusion and convection coefficients. When only a short period of time elapses before the search beam detects the particles, the change in velocity is small. In this case the transport of the ions will depend only on the local values of the diffusion and convection coefficients in velocity space. As is shown below, no assumptions about the velocity dependence is necessary.

Spatial diffusion affects, to some degree, all of the results. Once the tagged particles are created they are subject to diffusion across and along the field. Because of the symmetry of the experiment spatial diffusion along the field lines will not affect the results, but diffusion across the field does affect the outcome. Some percentage of the tagged particles will diffuse outside the laser beam and will no longer be counted as tagged particles. Since one would expect a link between spatial and velocity diffusion the loss of some particles out of the beam may leave behind a group of particles that behave differently. To estimate how big of an effect this is we have used the results of a previous experiment[25] where measurements of cross field spatial diffusion were made under conditions similar to those in this experiment. From the spatial diffusion paper, the FWHM of the tagged particle beams can be estimated from

$$\delta x^2_{\mathrm{FWHM}} \approx 2.77 D_\perp \delta t$$

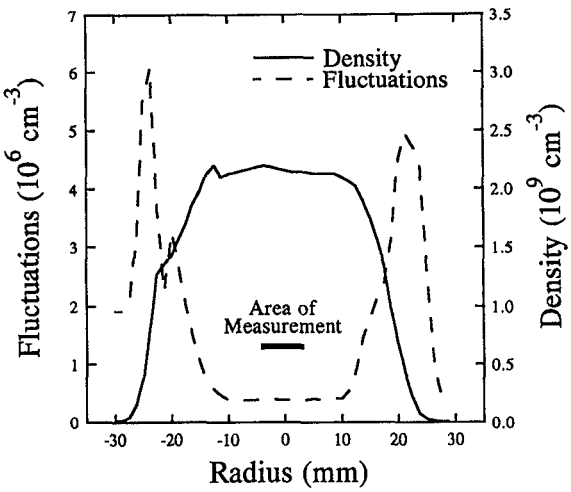

FIG. 4. The graph shows profiles of the density and density fluctuations (0.5–2.5 kHz) measured by Langmuir probes. The solid bar shows the area of the tagging measurements.

where $D_\perp = \rho_i \nu_{ii}$. Numbers typical of the current experiment are $n = 5\times10^9$ cm^{-3} and a magnetic field of 5 kG. This gives a $D_\perp$ of approximately 30 cm^2/s. The measurement time of 20 μs gives a change in the FWHM of less than 0.5 mm. The laser beam size was approximately 8 mm so that this is a small effect. The short-time results discussed below are almost free from the effects of spatial diffusion. This is further justification for ignoring spatial effects in the theory. Clearly as time goes on the effects of spatial diffusion mount. The loss of particles becomes evident in the long-time results presented below.

A. Quiet plasma short-time results

When the radial density profile of a Q-machine is virtually constant over the area of the ionizing hot plate, that area of the plasma can have a level of density fluctuations, $[\delta n/n]$ as low as 0.01%. Figure 4 shows the measured density profile and the profile of density fluctuations measured by a Langmuir probe. Drift waves were often seen on the edge of a Q-machine plasma column, several thermal ion Larmor radii away, radially, from the region of measurement. Note the 2 cm width in the center of the plasma column where the fluctuation level is less than 1%. This was the area (approximately 20 Larmor radii in diameter) in which all measurements cited as "quiet" plasma results were made. It was believed, due to previous work,[9] that classical collision processes would dominate. The laser beam was centered on this region. Very few ions that could have been influenced by the fluctuations on the edge of the profile would have had time to make their way into the probing laser beam area during the time of the measurement.

The results shown in this section were calculated from data that were taken over a short time scale (the time between measurements was much less than t_d and t_c). Ten μs windows were used for both the tagging laser beam and the search laser beam. The pulse sequence shown in Fig. 2 was used. Each data point required two separate measurements. The first measurement had a 0 μs time delay between the

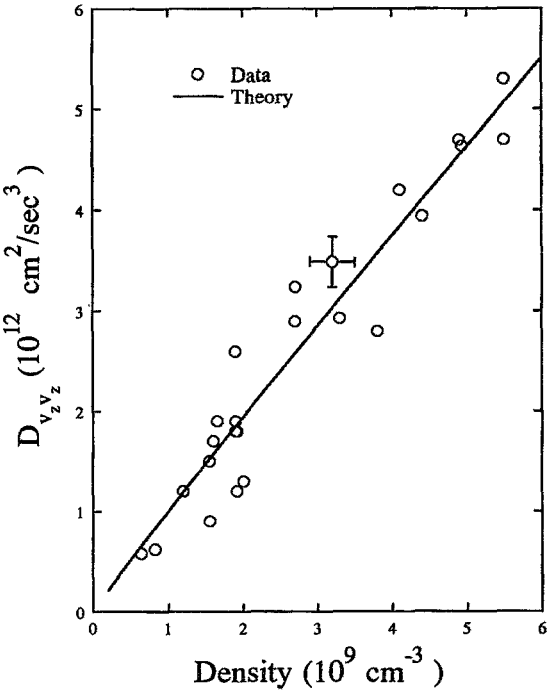

FIG. 5. Density dependence of diffusion in a quiet plasma. Theory is provided by Eq. (10). Here $n=1.4\times10^9$ cm^{-3} and $T=0.17$ eV. The tagging velocity is 0 cm/s in the plasma rest frame.

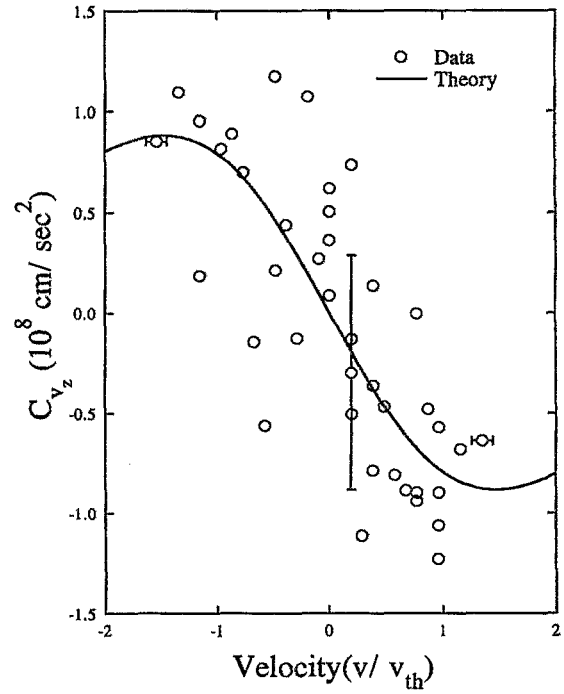

FIG. 6. Velocity space convection as a function of the tagged particles' initial velocity. Theory is provided by Eq. (9). Here $T_i = T_e=0.17$ eV and $n=1.4\times10^9$ cm^{-3}.

start of the tag beam and the start of the search beam, the second measurement had a delay of 10 μs. The average time between the creation of the tagged particles and detection by the search beam, were 5 and 15 μs, respectively, for the separate measurements. Each measurement resulted in data similar to that shown in Fig. 3. The data were then interpreted as explained above.

This timing sequence was the shortest that could be used due to signal-to-noise limitations. When the tagging and search pulse are the same length the signal level of the tagged particles is proportional to the square of the length of the pulse. This is because the signal is dependent on the number of particles created (proportional to the pulse length) and on the number of tagged particles seen (again proportional to the pulse length).

Equations (9) and (10) show that classical convection and diffusion depend on several variables that can be controlled experimentally. Namely, they depend on the field particles' temperature and density and the test particle velocity. The classical diffusion should depend linearly on the density. This is due simply to the increased number of collision centers present. Figure 5 shows the measured and theoretical [Eq. (10)] density dependence of the diffusion in a quiet plasma. The experimental data are not scaled to fit the theoretical prediction. The observed density dependence of the diffusion coefficient varies linearly with the density over the range of densities tested. The measured diffusion values agree with the theoretical prediction both in magnitude and density dependence.

Both the diffusion and convection coefficients should depend on the initial velocity of the tagged particles. A sequence of measurements was taken at several tagging laser frequencies and, therefore, initial tagged-particle velocities. These measurements were taken with tagged-particle velocities roughly within the range $\pm v_{\rm th}$.

Figure 6 shows the velocity dependence of the convection coefficient. The theory curve is found by plotting Eq. (9). The data show substantial spread and some data points are more than 3 times higher than expected from theory. Additionally, some data points have the wrong sign. The reasons for this inconsistency are discussed below. Overall, the data show a dependence in general agreement with the theory both in magnitude and sign as a function of velocity

Physically, the velocity dependence of the convection coefficient is, interpreted in the following way: In the plasma reference frame, particles are pushed by collisions towards slower speeds. That is, drag slows a particle's speed. This drag can be more clearly envisioned by considering the slope of the field-particle distribution function. Consider a particle moving with the average speed for all particles. This particle would have a speed $v=0$ in the plasma rest frame. There will be an equal number of particles moving to the right and to the left (zero slope) hence, the net result of the collisions produces no convection at this speed. In the rest frame of a particle with a positive speed (negative slope) there are more particles with negative relative speed than positive and thus collisions tend to, on average, reduce the particle's speed. The reverse is true for particles moving at speeds less than the average particle speed.

The diffusion coefficient, on the other hand, is an even function in speed. Particles random walk in velocity space and tend to move away from the center of the distribution.

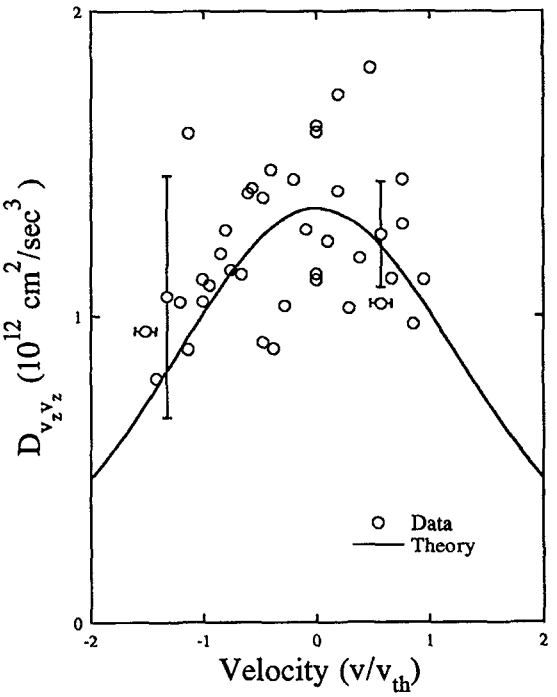

FIG. 7. Velocity space diffusion as a function of the tagged particle's initial velocity. Theory is provided by Eq. (10). Here $T_i = T_e = 0.17$ eV and $n = 1.4\times10^9$ cm^{-3}. The larger vertical error bar signifies repeatability. The other indicates a calculation error.

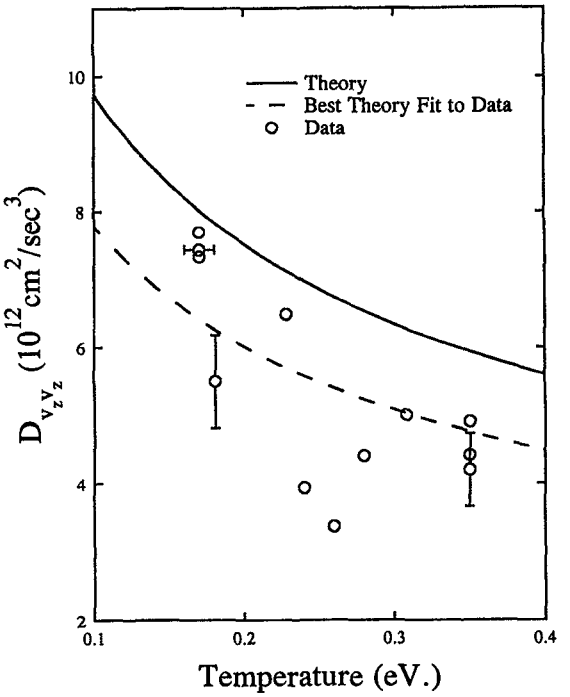

FIG. 8. Velocity space diffusion as a function of background particle temperature. Measured density $=8\times10^9$ cm^{-3}. The density for the best fit curve is 6×10^9 cm^{-3}.

The predicted velocity dependence of the Coulomb cross section should cause the diffusion to peak at zero velocity in the plasma frame and reduce with increasing velocity. The combination of the effects of convection pushing particles toward the distribution center and diffusion pushing particles away from it maintains the Maxwellian shape when the ions are in thermodynamic equilibrium.

Figure 7 shows the velocity dependence of the diffusion coefficient. The theory curve is found by plotting Eq. (10). All points but one are within a factor of 2 of that expected by theory without any normalization of theory to experiment. In fact, all but a few points are within 25% of the theory.

A comparison of the results of the diffusion and convection measurements shows that the precision of the diffusion measurement is superior. It is believed that the cause of the inferior precision of the convection coefficient was the magnitude of the relative drift of the frequency of the lasers in comparison to the change in average velocity of the test particle distribution. The drift of the laser is rated at less than 100 MHz/hour, however, it was difficult to measure precisely and thus, the exact drift rate is unknown. Since the convection is dependent on the first moment (position) of the data it is very susceptible to laser drift error. It is possible to estimate the error that this drift may have caused. For example, each measurement took approximately 5 minutes. Over this length of time the laser may have drifted 8 MHz, according to its specification. This drift alone would result in a change in the position of the first moment of roughly 500 cm/s. The convection is typically 1×10^8 cm/s^2 and the time of the measurement is 1×10^{-5}. Thus, it is thought that the change in the position of the first moment due to collisions would be $1\times10^8\times1\times10^{-5}=1000$ cm/s. Thus laser drift alone could account for as much as 50% of the measured convection. The diffusion measurement was not as sensitive to the drift because it is dependent only on the spread (or $\overline{v^2}$) in the tagged-particle distribution and not at all on the first moment.

The convection and diffusion coefficients depend on the thermal velocity of the background plasma. As the background temperature increases the average Coulomb collision cross section goes down and, thus, the convection and diffusion decrease. The values of the convection coefficient were so small that their measurements suffered from substantial uncertainties. With increasing temperature the convection would decrease, making the measurement even more difficult. Therefore, a measurement of the temperature dependence of the convection was not attempted.

To test this aspect of the theory the plasma was heated by introducing large amplitude EIC waves. The waves were created by the parametric decay of large amplitude, antenna launched lower hybrid waves.[25,9] The plasma density was 8.0×10^9 cm^{-3}. A 200 μs pulse of EIC waves was followed by a delay of 400 μs. The measurement of the transport was then made as previously discussed. The time between 90° collisions at this density and temperature is on the order of 100 μs. Using these parameters allowed the parallel and perpendicular temperatures to equilibrate.

Figure 8 shows the temperature dependence of the diffusion coefficient. The solid line is that expected by theory [Eq. (10)]. The gap between the data and the theory is most likely due to an error in the density reading. The dashed line

is the result of a least-square fit of the theory curve to the data points [that is the density in Eq. (10) was adjusted to give the best fit to the data]. The best fit density is 6×10^9 cm^{-3}. This difference is approximately 25%. The general decline with temperature is in the same direction as that expected from the theory although the spread in the data and its limited range do not allow this result to lead to a claim of substantial agreement with this aspect of theory, although, the results are consistent with theory.

The diffusion coefficient has the expected magnitude when compared to theory and the correct dependence on density, test particle velocity. The diffusion coefficient is consistent field particle thermal temperature dependence. The convection coefficient is found to be consistent with theory in magnitude, sign, and test particle velocity dependence. The quantitative dependence on test particle velocity of the convection coefficient is not clearly established by the experimental data although there is qualitative agreement. In a quiet plasma the measured velocity space transport, in the direction parallel to the magnetic field, is consistent with classical predictions for times much less than the 90° collision time.

B. Quiet plasma long-time results

The magnitude and velocity and temperature dependence of the diffusion coefficients and the magnitude and velocity dependence of the convection coefficient have been shown to be consistent with classical theory in the short-time-scale regime. In this section data are presented which indicate that these coefficients can also predict the long-time relaxation of the test particle distribution function. The long-time results are found from data where the time between measurements is as long as 160 μs. This time is on the order of t_d but still less than t_c. The long-time measurements could be used to get more accurate values for the magnitudes of the diffusion and convection coefficients, given that the velocity dependence is now established. However, we do not attempt that measurement here.

The long-time results were obtained by using the pulse sequence shown in Fig. 2. A series of scans was taken, with each new scan increasing the time delay t_m between the beginning of the tag pulse and the beginning of the search pulse. The value of t_m ranged from 10 to as much as 160 μs, and was increased in steps of 20 μs.

The results of these measured scans were predicted using the numerical method described in the Appendix. The first scan, which resulted from using a value for t_m of 10 μs, was entered as the initial distribution. The shape of the distribution at subsequent 20 μs intervals was then predicted using the computer program.

The area under the curve of the measured distribution is not conserved as it is in the computer model. In addition to the spatial diffusion of particles out of the laser beam extent, there are other reasons, such as divergence and lack of coalignment of the laser beams that contribute to the loss of signal. This loss of signal is not accounted for in the numerical method, therefore, the predicted distributions are scaled to the measured distributions so that the areas under the curves are identical.

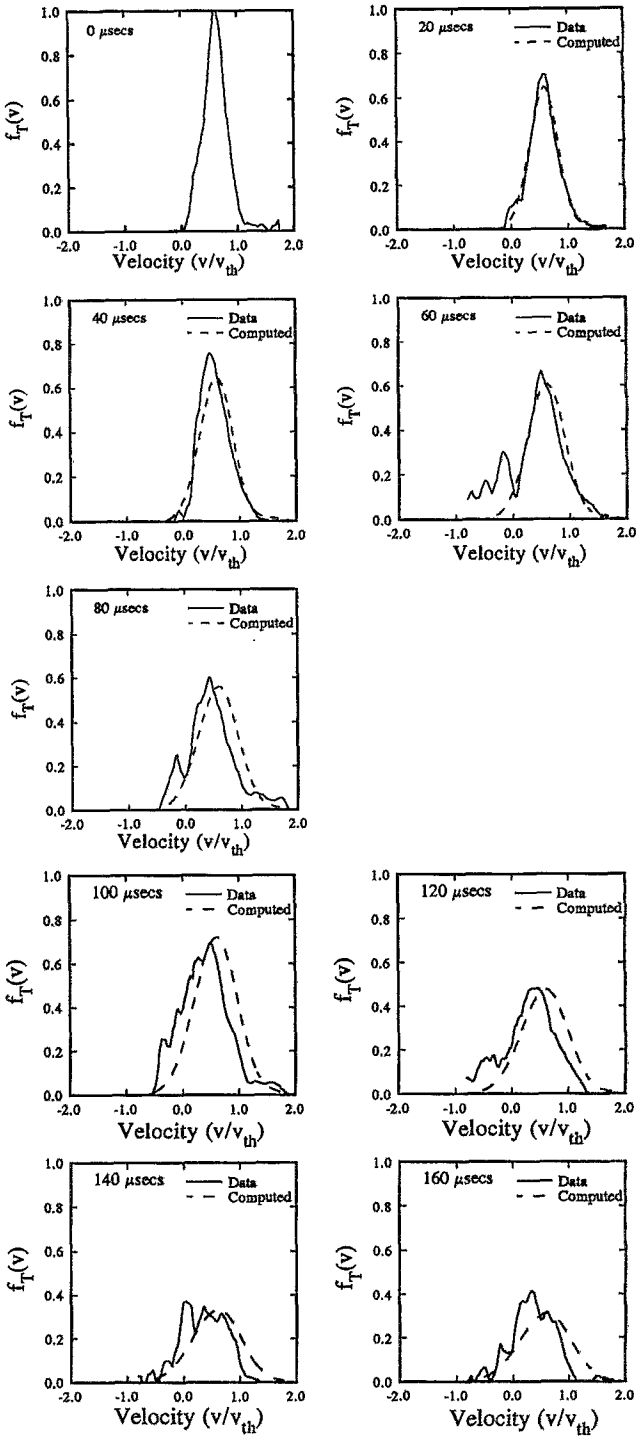

FIG. 9. Long-time behavior of test particle distribution compared with computer solutions to Eq. (11). The test particles were started with an average velocity of $0.7v_{th}$. Values of t_m are noted.

In the example shown in Fig. 9 the particles were started with a drift velocity of approximately $v=0.7v_{th}$. This example shows general agreement concerning the diffusion of the test particle distribution over the length of the measurement. The convection of the distribution, however, does not fit the predictions as well. Note the increasing difference between the theory and data concerning the convection. This

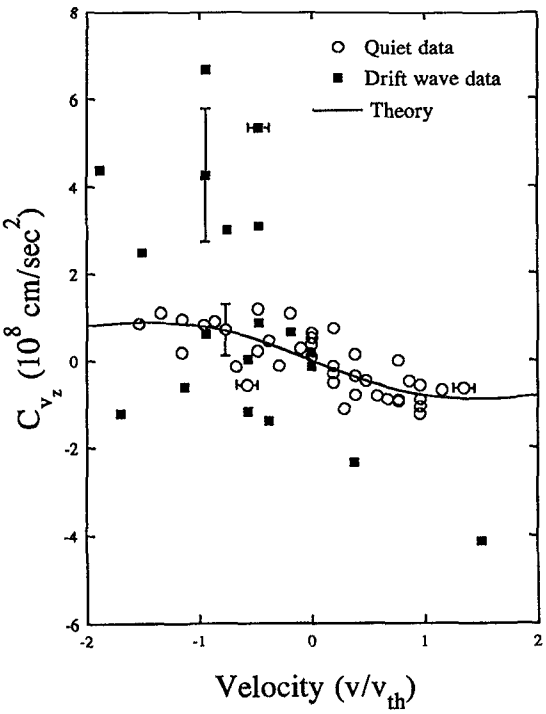

FIG. 10. Convection coefficients measured in the presence of drift waves and in a quiescent plasma.

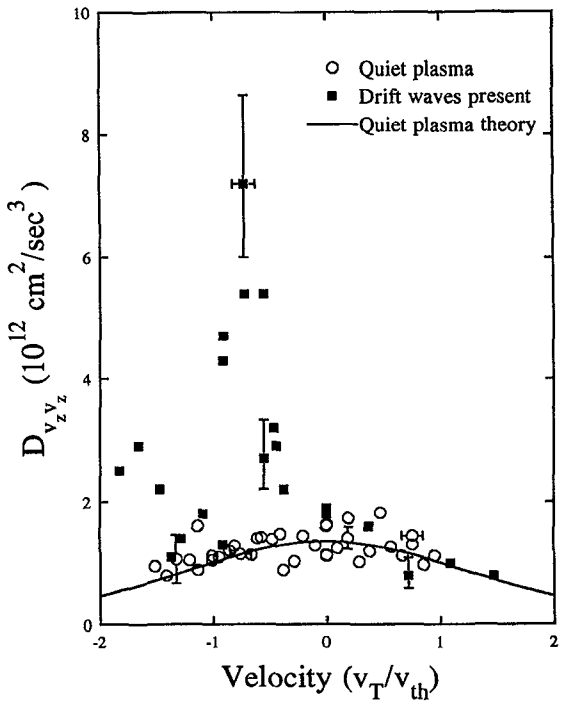

FIG. 11. Diffusion coefficients measured in the presence of drift waves. Open circles are data from a quiescent plasma.

is a result of the drift of the lasers and the time it took to complete the measurement. It should be remembered that the data are presented in the form in which they were taken. No smoothing or other alterations have been made.

More accurate measurements of the value of the convection coefficient could be made by taking two measurements separated by roughly 100 μs. Then, using the computer program, a value of the magnitude of the convection coefficient could be fitted to the data. This value would be more accurate than the short-time method since the expected convection would now be substantially larger than the error due to laser drift. However, this method requires independent knowledge of the velocity dependence of the convection coefficient.

C. Plasmas with fluctuations

When the density profile is not flat but instead has a density gradient, drift waves may be present. In a particular case when this happened the value of $\delta n/\delta x$ was 1.3×10^{10} cm^{-4} in the center of the plasma column where the tagging measurements were made. The total fluctuation level ($\delta n/n$) was measured to be 6% RMS. The wave was identified as a drift wave by the $1/B$ dependence of the frequency. During the measurement the peak frequency of the wave was 1500 Hz.

Figure 10 shows the convection measured in the presence of drift waves. The large scatter in the points shows that convection clearly is not classical.

Figure 11 shows the results of repeating the measurements of the diffusion coefficient for this case. The peak in diffusion at $v=-0.7v_{\rm th}$ was repeatable. Additionally, considering the error bars this peak indicated an increase of a factor of 5 to 10 over classical predictions. A direct causal relationship between the drift wave and this diffusion coefficient peak has not been found.

The presence of fluctuations leads to the consideration of several time scales. One of these scales is the autocorrelation time, τ_{ac}, which can be estimated from[26]

$$\tau_{ac}=|k\Delta(\omega/k)|^{-1}. \tag{16}$$

This is the approximate time required for a particle, traveling at the wave phase velocity, to cross the wave packet. Using the measured frequency spectrum and knowledge of the drift wave dispersion relation the autocorrelation is estimated to be on the order of 5 ms.

Other time scales of interest are the wave period and the measurement time. The wave period τ_w is 670 μs and the measurement time τ_{mt} is 20 μs. Physically, this ordering of time scales, $\tau_{ac}\gg\tau_w\gg\tau_{mt}$, means that the particles might be viewed as candidates for trapping in a single wave for the length of the measurement. The wave structure does not change significantly during the measurement time.

For quasilinear theory to be applicable the ordering would have to be $\tau_{mt}\gg\tau_{ac}$. This is not the case for these results.

It may be possible that the peak in Fig. 11 is simply due to reversible motion of the particles caught in the drift wave. If in fact this drift wave was causing the increase in phase space excursion in a resonant manner, then the parallel wavelength would be 25 cm. However, the 20 μs measurement time is much too small to see this type of resonant behavior. The measurement time would need to be on the order of the wave period in order to see this effect.

V. CONCLUSIONS

The development of new diagnostic tools often enables one to gain new insights into the physical processes being studied. The work described in this paper was made possible by the continuing development of the method of optical tagging and laser-induced fluorescence over the last decade.

This work has described the direct measurement of the velocity space transport coefficients for a fully ionized ion–electron plasma. The results obtained under quiet plasma conditions have been shown to be in agreement with classical collision theory. While classical collision theory was worked out decades ago, only in the last few years have experimental techniques developed to where the predictions could be verified to a good degree of accuracy.

In particular, in a quiet plasma, the velocity space diffusion coefficients were found to have the magnitude and velocity dependence predicted by classical theory. The temperature dependence of the diffusion coefficients was found to be consistent with the theory. The velocity space convection coefficients were found to have the predicted magnitude and velocity dependence within experimental resolution. Further, the data cited as long-time showed that the classical theory could predict the diffusion of the test particle distribution for up to 20% of the 90° collision time. The results with the drift wave present show that classical predictions do not hold for this case, the mechanism for the wave–particle interaction has not yet been resolved. Work on this aspect using the techniques described in this paper is continuing.

ACKNOWLEDGMENTS

The authors would like to acknowledge valuable inputs from Drs. Carl Oberman, Norman Rostoker, and Amiram Ron. They would also like to acknowledge the help of David Newsham, David Parsons, and Thomas Ross in taking the measurements. Additionally, the authors would like to thank the reviewer for making a number of suggestions that significantly improved the clarity of presentation of this paper.

This work was supported by National Science Foundation Grant No. PHY90-24667.

APPENDIX: COMPUTER MODEL OF ION TRANSPORT

There are several ways of solving partial differential equations by numerical methods. Some of these methods have been detailed in books by Ames[27] and by Smith.[28] The method of finite differences was used to solve Eq. (11). Following Ames and writing Eq. (11) in quasilinear form gives,

$$\frac{\partial^2 f(v)}{\partial v^2}+\frac{1}{D_{vv}}\left(C_v+2\frac{\partial D_{vv}}{\partial v}\right)\frac{\partial f(v)}{\partial v}+\frac{1}{D_{vv}}\left(\frac{\partial C_v}{\partial v}+\frac{\partial^2 D_{vv}}{\partial v^2}\right)f(v)=\frac{1}{D_{vv}}\frac{\partial f}{\partial t}. \tag{A1}$$

The implicit difference equation for this equation may be written

$$\frac{1}{h^2}\delta_v^2 U_{i,j+1}+\frac{1}{2h}M\mu\delta_v U_{i,j+1}+NU_{i,j}=\frac{P}{k}(U_{i,j+1}-U_{i,j}) \tag{A2}$$

where

$$h=\Delta v,\quad k=\Delta t,$$

$$\delta_v^2 U_{i,j}=U_{i+1,j}-2U_{i,j}+U_{i-1,j},$$

$$\mu\delta_v U_{i,j}=\tfrac{1}{2}(U_{i+1,j}-U_{i-1,j}),$$

$$M=\frac{1}{D_{vv}}\left(C_v+2\frac{\partial D_{vv}}{\partial v}\right),\quad N=\frac{1}{D_{vv}}\left(\frac{\partial C_v}{\partial v}+\frac{\partial^2 D_{vv}}{\partial v^2}\right),$$

$$P=\frac{1}{D_{vv}},\quad U_{i,j}=f_{i,j}+\Theta(h^2,k^2).$$

Here the first subscript refers to the space step and the second subscript to the time step. U refers to the approximate solution of $f(v)$ obtained using this method. Equation (A2) may be written, after collecting terms, as

$$U_{i+1,j+1}\left(\frac{1}{h^2}+\frac{M}{4h}\right)+U_{i,j+1}\left(\frac{-2}{h^2}-\frac{2P}{k}\right)+U_{i-1,j+1}\left(\frac{1}{h^2}-\frac{M}{4h}\right)=U_{i,j}\left(\frac{P}{k}-N\right). \tag{A3}$$

This system of equations is tridiagonal (meaning that when written in matrix form only the main diagonal and one subdiagonal above and below the main diagonal have nonzero elements) and is linear. The solution for the next time step is obtained by first using Gaussian elimination on the matrix to eliminate the lower subdiagonal. Then backward substitution is used to find the value of U_i at the $j+1$ time step. This process is called the Thomas algorithm.[27]

Typically, the velocity interval over which the integration was performed was divided into 128 intervals. This velocity interval was set to be approximately equal to the velocity resolution of the laser system. The time step was set at 1×10^{-7} s. This time step is 1% of the time that the tagging and search beams were on. A smaller time step did not result in any change in the output of the program.

[1] J. Bowles, R. McWilliams, and N. Rynn, Phys. Rev. Lett. **68**, 1144 (1992).
[2] N. Rynn, Rev. Sci. Instrum. **35**, 40 (1964); the UCI Q-machine is similar to that described in this reference.
[3] M. Rosenbluth, W. MacDonald, and D. Judd, Phys. Rev. **107**, 1 (1957).
[4] N. Rostoker, Nucl. Fusion **1**, 101 (1961).
[5] W. B. Thompson and J. Hubbard, Rev. Mod. Phys. **32**, 714 (1960).
[6] N. Rostoker and M. N. Rosenbluth, Phys. Fluids **3**, 1 (1960).
[7] D. N. Hill, S. Fornaca, and M. G. Wickham, Rev. Sci. Instrum. **54**, 309 (1983).
[8] R. Stern, D. Hill, and N. Rynn, Phys. Lett. A **93**, 127 (1983).
[9] R. McWilliams, M. Okubo, and N. Wolf, Phys. Fluids B **2**, 523 (1990).
[10] F. Skiff, F. Anderegg, T. N. Good, P. J. Paris, M. Q. Tran, N. Rynn, and R. A. Stern, Phys. Rev. Lett. **61**, 2034 (1988).
[11] A. Fasoli, T. Good, F. Anderegg, F. Skiff, P. Paris, M. Tran, and M. Yamada, Phys. Rev. Lett. **63**, 2052 (1989).
[12] A. Fasoli, F. Skiff, T. Good, and P. Paris, Phys. Rev. Lett. **68**, 2925 (1992).
[13] A. Hyatt, C. Driscoll, and J. Malmberg, **59**, 2975 (1987).
[14] M. Ono, Rev. Sci. Instrum. **42**, (1979).
[15] R. Fisher and R. Gould, Phys. Fluids **14**, 57 (1971).
[16] R. McWilliams and R. Motley, Phys. Fluids **24**, 2022 (1981).

[17]R. Schneider and G. Werth, Z. Phys. A **293**, 103 (1979).
[18]F. Skiff, T. Good, F. Anderegg, and P. Paris, Phys. Lett. A **137**, 57 (1989).
[19]P. Pappas, M. Burns, D. Hinshelwood, M. Feld, and D. E. Murnick, Phys. Rev. A **21**, 1955 (1980).
[20]W. MacDonald, M. Rosenbluth, and W. Chuck, Phys. Rev. **107**, 350 (1957).
[21]F. Hinton, in *Handbook of Plasma Physics*, edited by M. Rosenbluth and R. Sagdeev (North-Holland, New York, 1983), Vol. 1, p. 147, and references within.
[22]S. Ichimaru, in *Plasma Physics: An Introduction to Statistical Physics of Charged Particles* (Benjamin/Cummings, Menlo Park, 1986), Chap. 1, p. 9.
[23]B. A. Trubnikov, in *Reviews of Plasma Physics*, edited by M. Leontovich (Consultants Bureau, New York, 1965), Vol. 1, Chap. 2.
[24]D. Montgomery and D. Tidman, in *Plasma Kinetic Theory* (McGraw-Hill, New York, 1964), Chap. 1.
[25]R. McWilliams and M. Okubo, Phys. Fluids **30**, 2849 (1987).
[26]R. Davidson, in *Methods in Nonlinear Plasma Theory* (Academic, New York, 1972), Chap. 4.
[27]W. F. Ames, *Numerical Methods for Partial Differential Equations, Computer Science and Applied Mathematics*, 2nd ed. (Academic, New York, 1977).
[28]G. Smith, *Numerical Solution of Partial Differential Equations: Finite Difference Methods*, Oxford Applied Mathematics and Computing Science Series, 3rd ed. (Clarendon, New York, 1985).